Nuclear Magnetic Resonance and ab Initio Studies of Small Complexes Formed between Water and Pyridine Derivatives in Solid and Liquid Phases

Shasad Sharif,[†] Ilja G. Shenderovich,*[,†,‡] Leticia González,[†] Gleb S. Denisov,[‡] David N. Silverman,[§] and Hans-Heinrich Limbach*[,†]

Institut für Chemie und Biochemie, Freie Universität Berlin, Takustrasse 3, D-14195 Berlin, Germany, Institute of Physics, St. Petersburg State University, 198504 St. Petersburg, Russian Federation, and University of Florida, Box 100267 Health Center, Gainesville, Florida 32610-0267

Received: March 2, 2007; In Final Form: April 27, 2007

The structure and geometry of hydrogen-bonded complexes formed between heterocyclic bases, namely, pyridine and 2,4,6-trimethylpyridine (collidine), and water were experimentally studied by NMR spectroscopy in frozen phase and in highly polar aprotic liquefied freon mixtures and theoretically modeled for gas phase. Hydrogen-bonded species in frozen heterocycle−water mixtures were characterized experimentally using ^{15}N NMR. When base was in excess, one water molecule was symmetrically bonded to two heterocyclic molecules. This complex was characterized by the r_{HN} distances of 1.82 Å for pyridine and 1.92 Å for collidine. The proton-donating ability of water in such complexes was affected by an anticooperative interaction between the two coupled hydrogen bonds and exhibited an apparent pK_a value of about 6.0. When water was in excess, it formed water clusters hydrogen bonded to base. Theoretical analysis of binding energies of small model heterocycle−water clusters indicated that water in such clusters was oriented as a chain. The NMR estimated r_{HN} distances in these species were 1.69 Å for pyridine and 1.64 Å for collidine. Here, the proton-donating ability of the hydroxyl group bonded to the heterocycle was affected by a mutual cooperative interaction with other water molecules in the chain and became comparable to the proton-donating ability of a fictitious acid, exhibiting an apparent pK_a value of about 4.9. This value seems to depend only slightly on the length of the water chain and on the presence of another base at the other end of the chain if more than two water molecules are involved. Thus, the proton-donating ability of the outer hydroxyl groups of biologically relevant water bridges should be comparable to the proton-donating ability of a fictitious acid exhibiting a pK_a value of about 4.9 in water. Driven by the mixing entropy, monomeric water presented in the aprotic freonic mixtures above 170 K but completely precipitated upon further cooling. Traces of water could be suspended in the mixtures down to 130 K in the presence of about 20-fold excess of heterocyclic bases. The obtained experimental data indicated that at these conditions water trended to form the symmetric 2:1 heterocycle−water complexes, whose bridge protons resonated around 6.7 ppm.

Introduction

Medium- and long-range proton transport assisted by water bridges is part of many biological processes.[1−3] For example, it is well-founded that in one of the most investigated enzymes, namely, carbonic anhydrase II,[4,5] a bridge formed by several water molecules provides an enormously efficient proton transfer inside the enzyme's active site cavity. The rate constant of this process is up to 10^6 transfers per second. In the wild-type carbonic anhydrase II, the proton transfer taking place between the Zn-bound hydroxyl or water and the bulk water is shuttled by imidazole of His-64, which is located close to the entrance of the active site cavity; shown in Scheme 1 is the assumed structure of the water bridge.[1,6] While the overall mechanism of the catalytic activity of this enzyme was extensively studied and was supposed to be well understood,[7,8] it was difficult to locate these water bridges by the presently available experimental techniques.[9] Theoretical studies of this phenomenon indicated that although a water bridge made a substantial contribution to the proton transport, its formation probability is low.[1] Hence, it is questionable how this proton transfer is realized in nature, what is the proton-donating ability of the outer water molecules in such a water bridge, and how it depends on the number of water molecules involved in the bridge. The main goal of this paper is to inspect interactions between water and model bases, aiming at predicting properties of water bridges in biological systems.

SCHEME 1: Shown Is the Assumed Water Bridge Structure in the Wild-Type Carbonic Anhydrase II between the Zn Center and the HIS-64, Adapted from Ref 1

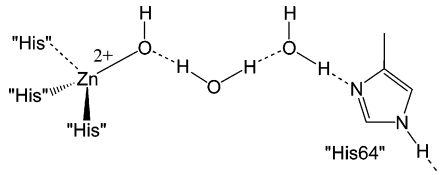

Recently, experimental and theoretical studies of benzene−[10−14] and phenol−water[15−18] clusters predicted that their topology

* To whom correspondence should be addressed. (I.G.S.) Tel: +49 30 8385 3615. E-mail: shender@chemie.fu-berlin.de. (H.-H.L.) Tel: +49 30 8385 5375. Fax: +49 30 8385 5310. E-mail: limbach@chemie.fu-berlin.de.
[†] Freie Universität Berlin.
[‡] St. Petersburg State University.
[§] University of Florida.

10.1021/jp071725t CCC: $37.00
Published on Web 06/19/2007

deviated from the corresponding pure water clusters and was determined by the dominate interaction between the aromatic systems and the water in the cluster. For the phenol−water clusters, it was found as a dominant interaction in the conventional hydrogen bonds with one hydroxyl replaced by a phenolic group and for the benzene−water cluster in the π-hydrogen-bonding interaction.[10−18] In contrast, when water interacted with a strong proton acceptor, namely, pyridine, the conventional hydrogen bonding should become the dominant interaction. The strength of this interaction will increase upon methyl substitution of pyridine.[19] Spectral features observed in Fourier transform infrared (FT-IR) spectra of aprotic dilute solutions of water and pyridine derivatives were interpreted as indicative of formation of the simplest 1:1 hydrogen-bonded species and symmetrical 2:1 species where one water was bridged between two pyridines.[20,21] At higher water concentrations, the presence of less defined aggregates, which presumably contained several water molecules bonded to pyridine, has been suggested. However, these structures were only assumed or predicted theoretically, but the hydrogen bond geometries were not defined experimentally. This can be done using the method tested in previous studies for various complexes between carboxylic acid and pyridine and its derivative collidine (2,4,6-trimethylpyridine) with the help of NMR spectroscopy.[22−25] The method is based on a correlation established between the ^{15}N chemical shifts and the geometries of the corresponding H-bonds.[26−29] Reliability of geometries obtained using this method was supported in a number of top-level theoretical calculations.[30−34]

Thus, the present study examines the feasibility of using variable temperature high-resolution liquid- and solid-state NMR spectroscopies to analyze biologically relevant hydrogen-bonding interactions between water and heterocyclic bases. Pyridine and collidine were selected as model bases due to their optimal properties required for the probe molecules in NMR and simplicity of forming hydrogen bonds. The main goal of this work, experimental simulation and property analyses of water bridges, was subdivided in the following three aims: (i) to inspect using ^{1}H and ^{15}N liquid-state NMR whether water bridges can be formed and studied in aprotic environments; (ii) to investigate using ^{15}N solid-state NMR the proton-donating ability of the outer water molecules in water bridges and its dependence on the number of water molecules involved in the bridges in frozen phase; and (iii) to determine the most energetically preferable structures of small heterocyclic base−water clusters of different composition using ab initio calculations.

This paper is organized as follows. After an Experimental and Theoretical section where the formalism of the data analysis is described, the results are reported and discussed.

Materials and Methods

Materials. ^{15}N-enriched (98%) pyridine, ^{15}N-enriched (95%) nitromethane, dichloromethane-d_2, and chloroform-d_1 were purchased from Deutero GmbH. ^{15}N-labeled collidine (2,4,6-trimethylpyridine) was synthesized from ^{15}N-enriched (95%) NH_4Cl (Deutero GmbH) and 2,4,6-trimethylpyrylium tetrafluoroborate (Lancaster).[35] The product was characterized by ^{1}H, ^{13}C, and ^{15}N liquid-state NMR. The deuterated freon gas mixture $CDF_3/CDClF_2$ for the low-temperature NMR experiments, whose composition varied between 1:2 and 1:3, was prepared from chloroform-d_1 by a modified recipe proposed by Siegel and Anet.[36] Details of the synthesis and properties of the freonic mixtures were reported recently.[37]

NMR Measurements. Solid-state spectra of the ^{15}N-labeled pyridine and collidine containing different quantities of water were performed at 30.41 MHz on a Bruker MSL 300 spectrometer (7 T) in the temperature range of 220 to 130 K. Standard cross-polarization ^{15}N $\{^{1}$H$\}$ CP NMR experiments were performed under magic angle spinning (MAS) conditions with a spinning rate of 6 kHz. The 90° pulse width was about 8 μs, the cross-polarization contact time was 5 ms, and the recycle time was 20 s. All spectra were referenced to external solid $^{15}NH_4Cl$ (95% ^{15}N-enriched).

Liquid-state ^{1}H and ^{15}N NMR spectra were measured using a Bruker AMX 500 spectrometer (500.13 MHz for ^{1}H, 50.68 MHz for ^{15}N) equipped for low-temperature NMR down to 100 K. The solvent used was a liquefied deuterated freon gas mixture $CDF_3/CDClF_2$. The ^{1}H spectra were indirectly referenced to tetramethylsilane (TMS) by setting the central component of the residual $CHClF_2$ triplet in the freon mixture to 7.18 ppm.[37] Standard ^{1}H and inverse-gated ^{1}H-decoupled ^{15}N NMR spectra were recorded with recycle times of 3 and 5 s, respectively. To reference the ^{15}N chemical shifts in liquid state, we have recorded without ^{2}H field locking the ^{15}N spectra of neat nitromethane under the same field-locking condition as the deuterated liquefied freonic mixture. To convert the ^{15}N chemical shifts from the nitromethane scale into the solid external $^{15}NH_4Cl$ scale, the relation $\delta(CH_3NO_2, \text{liquid}) = \delta(^{15}NH_4Cl, \text{solid}) - 341.168$ ppm was used.[38]

NMR Samples. The solid-state sample preparations were done by filling a special glass insert with ^{15}N-enriched pyridine or collidine and defined quantities of water. The sealed insert was mounted into an NMR rotor and frozen out. ^{15}N CP MAS spectra were recorded at 220 to 130 K. The liquid-state samples were prepared by condensing the liquefied freonic gas mixture to 8 and 10 μL of pyridine or collidine, respectively, with defined quantities of water suspended in dichloromethane-d_2. ^{1}H and ^{15}N spectra of the pyridine− or collidine−water mixtures were recorded at 270 to 110 K; concentrations of pyridine and collidine were 0.16 and 0.14 mM, respectively.

Ab Initio Calculations. Theoretical calculations were performed using the second-order Møller−Plesset perturbation theory[39,40] (MP2) and density functional theory (DFT) with the B3LYP[41,42] functional, combined with the standard basis sets 6-31+G(d)[43] and 6-31+G(d,p),[43] respectively. After each geometry optimization, a calculation of the vibrational frequencies was performed to ensure that the calculated geometry corresponds to a minimum and not to a saddle point on the potential energy hypersurface.

Zero-point vibrational energy (ZPVE) corrections were included using harmonic frequencies evaluated at the MP2/6-31+G(d) and B3LYP/6-31+G(d,p) levels of theory. The geometry optimizations were followed by a single-point energy calculation using a more flexible basis set, namely, 6-311++G-(3df,2p)[44] or 6-311++G(d,p)[44] for DFT and MP2 levels, respectively; this leads to the protocols B3LYP/6-311++G-(3df,2p)//B3LYP/6-31+G(d,p) and MP2/6-311++G(d,p)//MP2/6-31+G(d), which are proved to achieve reliable accuracy in the calculation of the binding energies of hydrogen-bonded clusters.[45,46] The binding energy ΔE_e without ZPVE was calculated from the following relation,

$$\Delta E_e = E(\text{cluster}) - E(X_m) - E(W_n) \quad (1)$$

where the total energies are as follows: E(cluster) is the energy of the complete hydrogen-bonded cluster, $E(X_m)$ is the energy of the heterocyclic compound, with X = collidine or pyridine and m = 1 or 2, and $E(W_n)$ is the energy of the water clusters

with $n = 1$, 2, 3, or 6 water molecules optimized independently at the same level of theory. The basis set superposition error $\Delta\epsilon$(BSSE) to the binding energy was estimated using the counterpoise method of Boys and Bernardi.[47−49]

To investigate the bonding features of the hydrogen-bonded species, we used the atoms in molecules (AIM) theory of Bader.[50] Using this formalism, we located the bond critical points, that is, points where the electron density function, $\rho(r)$, was minimal along the bond path and maximal in the other two directions. The electron density increases with the hydrogen bond strength and hence gives useful information about the strength of the bond.[51]

To calculate the chemical shielding, the gauge independent atomic orbital (GIAO)[52] method approach was used at B3LYP/6-311++G(3df,2p) and MP2/6-311++G(d,p) levels of theory. The principal components of the calculated chemical shielding tensors were absolute shielding values, that is, were referenced to the shielding of the "bare" nucleus. The chemical shielding σ could be converted to chemical shift δ by the relation $\delta = A - \sigma$, where A is the absolute chemical shielding of the reference. The ^{1}H reference value for the chemical shielding is the proton shielding of methane CH_4 calculated at the same level of theory; the corresponding values are 31.44 (DFT) and 31.71 ppm (MP2). These values were then converted into TMS scale taking into account the experimental difference of 0.14 ppm.[53,54] The ^{15}N chemical shielding of the heterocyclic nitrogen was calculated to be −105.37 (DFT) and −110.82 ppm (MP2) for pyridine and −91.54 (DFT) and −87.31 ppm (MP2) for collidine. However, in this work, we were only interested in the relative values of the ^{15}N chemical shifts of the ring nitrogen; hence, we set the free pyridine and collidine to zero. The same procedures were also done for the experimentally obtained values.

All quantum chemical calculations of geometries, harmonic vibrations, total energies, and chemical shieldings were carried out with the GAUSSIAN98 program[55] on an Origin 3400 (SGI) computer with 36 processors MIPS R14000 and 20 Gigabytes of memory.

Theoretical Section

Geometric and NMR Hydrogen Bond Correlations. It has been shown that the valence bond orders defined by Pauling[56] are useful for describing geometric correlations of hydrogen bonds of the type A−H···B.[57,58] The bond valences p of the A−H and of the H···B bonds are defined as described below, and in the bond valence concept, it is assumed that the total bond order of hydrogen is unity[59]

$$p_1 + p_2 = 1 \text{ with } p_i = \exp\{-(r_i - r_i^\circ)/b_i\} \text{ where } i = 1, 2 \quad (2)$$

Here, $r_1 = r_{AH}$ represents the A···H distance, $r_2 = r_{HB}$ represents the H···B distance, and p_1 and p_2 are the corresponding valence bond orders. Whereas r_1° and r_2° represent the equilibrium distances in a fictitious free diatomic units AH and HB^+, b_1 and b_2 are the parameters describing the decays of the bond order when the bond is stretched. Therefore, it follows that r_1 and r_2 depend on each other. For OHN hydrogen bonds, Steiner[57] proposed the parameters set $r_{OH}^\circ = 0.942$ Å, $r_{HN}^\circ = 0.992$ Å, $b_{OH} = 0.371$ Å, and $b_{HN} = 0.385$ Å. Recently, it is shown that these equations were only valid for equilibrium geometries, as zero-point vibrations were not taken into account.[26] To take the latter ones into account, the following empirical bond order equations for the equilibrium bond orders were proposed

$$p_1 = p_1 - 360(p_1 \cdot p_2)^5 (p_1 - p_2) - 0.7(p_1 \cdot p_2)^2 = \exp\{-(r_1 - r_1^\circ)/b_1\}$$

$$p_2 = p_2 + 360(p_1 \cdot p_2)^5 (p_1 - p_2) - 0.7(p_1 \cdot p_2)^2 = \exp\{-(r_2 - r_2^\circ)/b_2\} \quad (3)$$

It was useful to express the correlation in terms of the hydrogen bond coordinates, defined as $q_1 = 1/2(r_1 - r_2)$ and $q_2 = r_1 + r_2$. In the linear case, q_1 represents the deviating proton distance from the hydrogen bond center and q_2 is the distance between the heavy atoms A and B, as indicated in Scheme 2. Note that the correlation is independent from the hydrogen bond angle. In this paper, A−H···B corresponds to the intermolecular OHN hydrogen bond formed between water molecules and heterocyclic bases; A is the oxygen of water, and B is the ring nitrogen of the base. The correlation curve[28] of q_2 vs q_1 is presented in Figure 7a (dotted line); it shows that when the proton is transferred from A to B, a hydrogen bond contraction occurs that is maximum when the proton is located approximately in the hydrogen bond center. To visualize the quantum effects, also the corrected[26] q_2 vs q_1 curve is presented in Figure 7a (solid line).

The bond order is also useful to correlate NMR parameters with hydrogen bond geometries.[26−28] The following relations were proposed for the chemical shifts of OHN hydrogen bonds[26]

$$\delta(\mathrm{OH}N) = \delta(N)^\circ p_{OH} + \delta(\mathrm{H}N)^\circ p_{HN} + 4\,\delta(\mathrm{OH}N)^*\, p_{OH} \cdot p_{HN} \quad (4)$$

$$\delta(\mathrm{O}H\mathrm{N}) = \delta(\mathrm{O}H)^\circ p_{OH} + \delta(H\mathrm{N})^\circ p_{HN} + 4\,\delta(\mathrm{O}H\mathrm{N})^*\, p_{OH} \cdot p_{HN} \quad (5)$$

Here $\delta(N)^\circ$, $\delta(\mathrm{H}N)^\circ$, $\delta(\mathrm{O}H)^\circ$, and $\delta(H\mathrm{N})^\circ$ represent the chemical shifts of the fictitious free molecular units into which the OHN hydrogen bond could formally dissociate. $\delta(\mathrm{OH}N)^*$ and $\delta(\mathrm{O}H\mathrm{N})^*$ are "excess" terms that describe the deviation of the quasi-symmetric hydrogen bond from the average of the fictitious limiting molecular units. These parameters were given in ref 26: $\delta(\mathrm{H}N)^\circ = 126$ ppm, $\delta(\mathrm{OH}N)^* = 0$ ppm, $\delta(N)^\circ = 0$ ppm, $\delta(H\mathrm{N})^\circ = 7$ ppm, $\delta(\mathrm{O}H\mathrm{N})^* = 20$ ppm, and $\delta(\mathrm{O}H)^\circ = 2$ ppm for complexes in liquid phase and $\delta(\mathrm{O}H)^\circ = -3$ ppm for complexes in solid phase.

The pK_a values associated to the bonding proton in collidine−acid complexes can be estimated from the q_1 value using the following equation:[28,29]

$$\mathrm{p}K_a = 2.8 - 7q_1 \quad (6)$$

Results

NMR Spectroscopy. The results of NMR experiments are depicted in Figures 1−3. The molecular structures are analyzed in Figures 4−7 and described partly in this section and in the discussion.

In Figure 1, low-temperature ^{1}H NMR spectra of a mixture of ^{15}N-labeled collidine with water dissolved in the liquefied freonic mixture are depicted. The spectra obtained for pyridine−water mixtures are qualitatively the same, and the interested reader can find them in the Supporting Information. We prefer to report in the main text the experimental data obtained for collidine since its hydrogen-bonded complexes were extensively studied in the past.

Upon cooling, water is partially frozen out, which significantly reduced its content in the solution. Without an acceptor,

SCHEME 2: Hydrogen Bridge, the Parameters Characterizing the Geometry: Distances r_{AH} and r_{BH} and the Angle ($\alpha = 180°$)

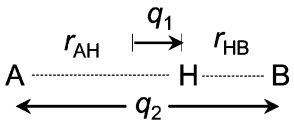

water completely precipitated from the solution below 170 K. In contrast, in the presence of collidine, water was observed in the solution down to 130 K in the whole temperature range. At 300 K, the water protons resonated at 2.8 ppm (Figure 1a). The water signal is getting significantly broader and is monotonically shifted to 4.6 ppm at 220 K (cf. Figure 1c). By further lowering the temperature, the water signal becomes sharp again. Cooling gives rise to an asymptotically approached low-field shift of the ^{1}H water signal up to 6.7 ppm at 130 K (Figure 1f). It was not possible to vary the relative content of water, because about 20-fold base excess was needed to suspend water in the mixture at lower temperatures.

^{15}N-labeled pyridine− or collidine−water mixtures were also studied in freonic mixtures at low temperatures by ^{15}N NMR. For pyridine in the presence of water, a sharp ^{15}N signal was observed at 271.4 (260 K) and 267.4 ppm (120 K). Similar results were recorded for collidine−water mixtures: The signal appeared at 259.6 (260 K) and 257.6 ppm (120 K). These ^{15}N chemical shifts are less informative because of the fast exchange between the free and the hydrogen-bonded heterocyclic bases. The ^{15}N NMR spectra in liquid state are therefore presented in the Supporting Information.

An overview of the ^{15}N spectra of mixtures of ^{15}N-labeled pyridine and water in the frozen state is presented in Figure 2. The water content in the mixtures increases from the top to the bottom. When pyridine is in excess, above the melting point of the 4:1 mixture, there is a fast exchange between the hydrogen bonded and the bulk pyridine. Thus, the corresponding spectrum displays the only averaged signal at 269 ppm whose chemical shift depends on the pyridine:water ratio (Figure 2a). When the exchange is suppressed in the frozen phase, the ^{15}N NMR spectrum displays two signals (Figure 2b). The signal at 275 ppm belongs to frozen pyridine,[28] and the one at 261 ppm belongs to some pyridine−water species. Upon an increase of the water content, the signal at 261 ppm became dominant while the intensity of the signal of bulk pyridine is strongly reduced (Figure 2c). When water is in excess, the spectra display the only signal at 255 ppm whose chemical shift does not depend measurably on the water content (Figure 2d).

Spectra obtained for a more basic pyridine derivative,[60] ^{15}N-enriched collidine, are depicted in Figure 3. Again, when the base is in excess, above the melting point of the 3:1 mixture, one observes the only averaged signal at 264 ppm (Figure 3a). In the frozen phase, this signal splits in two: The first one at 268 ppm corresponds to frozen bulk collidine,[28] and the second one at 257 ppm corresponds to collidine forming hydrogen-bonded species with water (Figure 3b). As long as the collidine:water ratio is above 2:1, the spectra contain exclusively these two signals. In contrast, when this ratio is below 1:2, the corresponding spectra display the only signal at 245 ppm (Figure 3e).

Theoretical Studies on Small Model Heterocycle−Water Clusters. To simplify the interpretation of experimental results, MP2 and DFT calculations on small model pyridine− and collidine−water clusters were performed. The resulting geometries of the collidine−water clusters are shown in Figure 4,

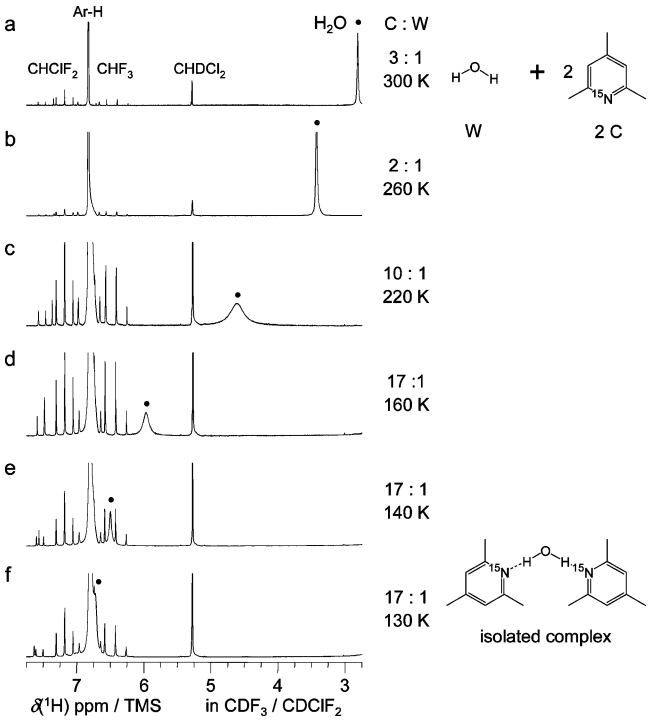

Figure 1. ^{1}H NMR liquid-state spectra of ^{15}N-labeled collidine−water complex in the freon mixture CDF_3/$CDClF_2$. The water signal (filled circle) appears at (a) 2.8, (b) 3.4, (c) 4.6, (d) 6.0, (e) 6.5, and (f) 6.7 ppm.

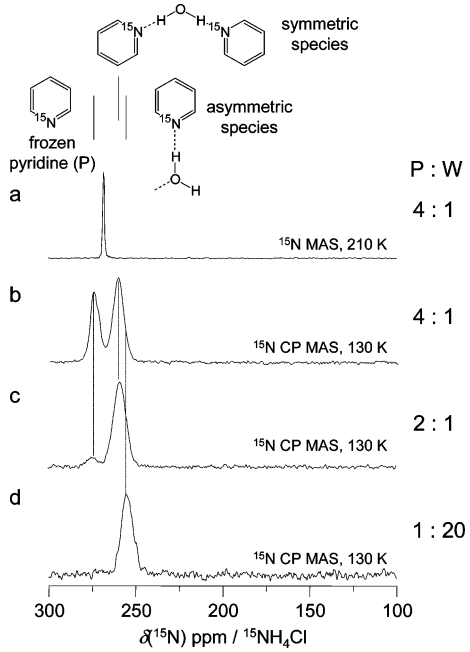

Figure 2. Solid-state spectra of ^{15}N-labeled pyridine−water mixtures at low temperatures. The ratios of pyridine to water are shown. (a) ^{15}N MAS NMR and (b−d) ^{15}N CP MAS NMR. All spectra were referenced to the external solid $^{15}NH_4Cl$. The peak positions are (a) 269 ± 1, where the signal is in exchange above the melting point of the mixtures, (b) 275 ± 1, (c) 261 ± 1, and (d) 255 ± 1 ppm.

and the hydrogen-bonded geometrical parameters were assembled in Table 1; further details for pyridine−water clusters can be found in the Supporting Information. Again, we prefer to focus on the data obtained for collidine.

As starting points for the optimization of heterocycle−water clusters, we used the most stable water cluster conformers.[61] We notice that the results of the hydrogen-bonded water clusters

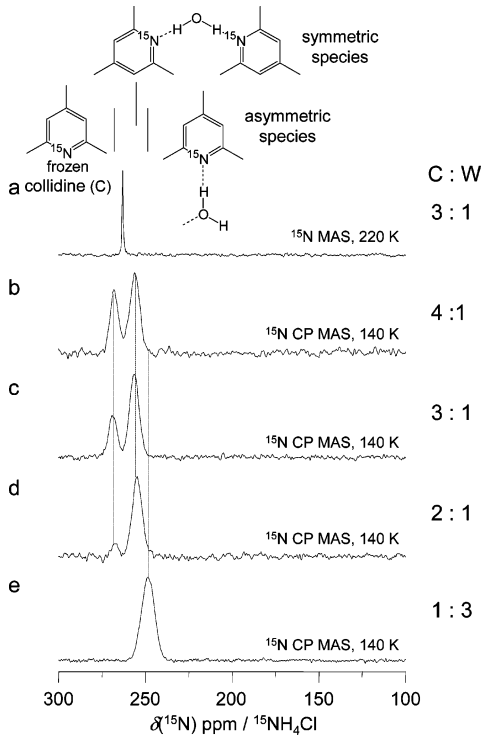

Figure 3. Solid-state spectra of ^{15}N-labeled collidine−water mixtures at low temperatures. The ratios of collidine to water are shown. (a) ^{15}N MAS NMR and (b−e) ^{15}N CP MAS NMR. All spectra were referenced to the external solid $^{15}NH_4Cl$. The peak positions are (a) 264 ± 1, where the signal is in exchange above the melting point of the mixtures, (b−d) 268 ± 1 and 257 ± 1, and (e) 245 ± 1 ppm.

obtained from DFT are qualitatively and quantitatively in agreement with those obtained from MP2. One exception is the CW21 cluster where the structures obtained with DFT and MP2 differ significantly: While DFT converged to a linear bridged structure, MP2 found a stacked cluster. It is a well-known feature of DFT that it does not account for dispersion interaction energy; hence, it is not surprising that is does not lead to a stacked structure, while MP2 does.[62,63] It should be mentioned, however, that a stacked structure for the similar cluster with pyridine (PW21) has not been found, neither at DFT nor at MP2 levels of theory. Moreover, the more flexible DFT structure of CW21 that has less tension of the OHN hydrogen bond angle (Table 1) seemed to be more realistic than a stacked structure; therefore, we consider the linear structure as the most probable one.

The binding energies with and without ZPVE corrections of the pyridine− and collidine−water clusters are visualized in Figure 5 and tabulated in Table 2. In the presence of water excess, the most stable structure among the calculated structures is the 1:3 cluster in which the three waters were clustered in a chain; see CW13C in Figure 4 and PW13C in the Supporting Information. Note that the conclusions obtained from this binding energy analysis are independent from the inclusion of the BSSE corrections to the binding energy. Similar trends are observed in light of the MP2 results. An exception, of course, constitutes the CW21 cluster since the DFT and MP2 calculations led to very different geometrical structures; therefore, the binding energies are very distinct. Note that after inclusion of the ZPVE, the binding energy of CW21 at MP2 level of theory becomes negative, indicating that this type of stacked cluster is indeed less stable. We have also performed the calculation at the DFT level of theory of a 2:6 cluster, where the water bridge was clustered as a chain; see CW26C in Figure 4 and PW26C in the Supporting Information. The binding energies of these clusters are further stabilized in comparison with the nonsaturated clusters PW13C and CW13C (cf. Table 2).

The binding energy trend is consistent with the geometry of the hydrogen bonds in the clusters, as reflected in the r_{HN} distances listed in Table 1. The shortest distance is found for the CW13C and CW26C clusters, followed by CW12, CW13R, and CW11. As expected, r_{HN} distances in the CW21 cluster are much longer than those in the other clusters due to the anticooperative interaction of the two hydrogen bonds. The strength of the hydrogen bonds can be also tracked by the electron density $\rho_{HN}(r)$ at the bond critical point of the N···H bond, the shorter (and stronger) the bond, the more charge was accumulated on the bond (Table 1); further details can be found in the Supporting Information.

GIAO calculations of the ^{1}H and ^{15}N chemical shifts of the heterocyclic nitrogen and the proton involved in the intermolecular OHN hydrogen bond were also performed. The values are listed in Table 1. To evaluate the quality of the DFT and MP2 calculations of the chemical shifts for protons and nitrogens, theoretical values are compared with the experimental ones. For nitrogen, we used the difference between the heterocyclic nitrogen in pyridine and collidine, which was $\Delta\delta(^{15}N) = 13.82$ and 23.51 ppm at DFT and MP2 level of theory, respectively. The experimental chemical shift difference of the frozen bases, pyridine and collidine, in solid state was found to be $\Delta\delta(^{15}N) = 7$ ppm.[28] Slight changes of $\Delta\delta(^{15}N)$ in liquefied freon mixture at 260 and 120 K were found, 11.1 and 10.5 ppm, respectively. The experimental ^{15}N chemical shift differences agree better with the theoretical value obtained from DFT. To evaluate the ^{1}H chemical shifts, we compared the theoretical and experimental values of the aromatic proton of collidine. From the calculations, values of 6.60 (DFT) and 6.36 ppm (MP2) are found. These values are in agreement with the experimental ones of 6.8 ppm in the freon mixture.

Discussion

Driven by the mixing entropy, monomeric water presents in the aprotic freonic mixtures above 170 K but completely precipitates upon further cooling. In contrast, traces of water can be suspended in the mixtures down to 130 K in the presence of an excess of heterocyclic bases. These water molecules are involved in a fast, on the NMR time-scale, exchange between different hydrogen-bonded species.

Two types of hydrogen-bonded heterocycle−water species were identified experimentally in the frozen phase. The first one was observed when the heterocyclic base was in excess while the second one was observed when water was in excess.

Theoretical studies of small model heterocycle−water clusters indicated that the most energetically preferable structure in such clusters was a hydrogen-bonded water bridge terminated on both ends with base molecules. When the base is in excess, this structure represents a 2:1 heterocycle−water cluster, where one water is coordinated to two bases. When water is in excess, this structure represents the longest possible water chain coordinated to two bases. In the following section, we will discuss and compare the obtained experimental and theoretical results in more detail.

Water−Base Complexes in Aprotic Environment. In an aprotic environment, protons of solitary water molecules resonate around 2 ppm while water microdrops give rise to a peak at 4.8 ppm typical for liquid water.[64] Water molecules involved in stronger hydrogen bonds are characterized by higher values of the ^{1}H chemical shift.

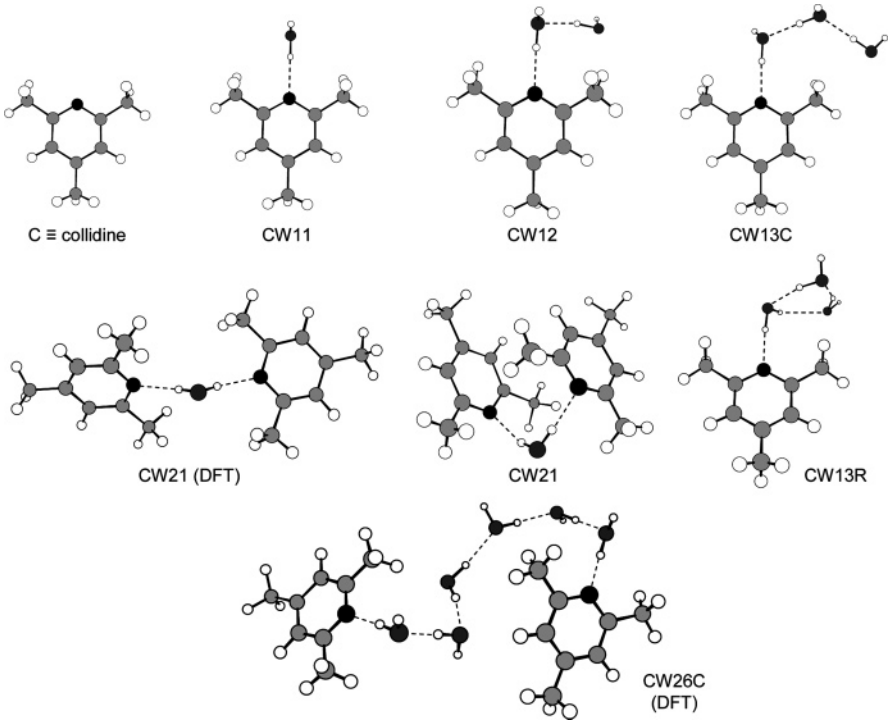

Figure 4. MP2/6-31+G(d) optimized structures of the collidine (C)−water (W) clusters investigated in this study. The numbers included on the label denote the proportion collidine:water; additionally, C stands for chain and R stands for ring. The DFT structures are qualitatively similar and therefore not shown, except for the CW21 and CW26C clusters.

TABLE 1: NMR and Selected Structural Hydrogen Bonds Parameters of Collidine−$(H_2O)_n$ Clusters with n = 0.5, 1, 2, 3, and 6 at DFT and the MP2 Level of Theory

collidine	n	r_{NH} (Å)	r_{OH} (Å)	r_{NO} (Å)	α(OHN) (°)	$\delta(^{15}N)^a$ (ppm)	$\delta(^1H)^b$ (ppm)	$\rho_{HN}(r)^c$
				B3LYP/6-311++G(2df,2p)//B3LYP/6-31+G(d,p)				
C	0					0		
CW21[d]	1/2	2.021 (2.019)	0.976 (0.976)	2.988 (2.987)	170.6 (171.1)	−12.42 (−12.74)	4.86 (4.88)	0.0256 (0.0258)
CW11	1	1.915	0.983	2.895	174.5	−18.84	6.15	0.0326
CW12	2	1.837	0.993	2.819	169.6	−25.22	8.05	0.0389
CW13C	3	1.784	0.999	2.781	174.8	−29.11	9.40	0.0429
CW13R	3	1.874	0.987	2.859	175.0	−21.91	7.23	0.0358
CW26C[d]	6	1.789	0.999	2.785	174.3	−29.24	9.34	
	6	(1.766)	(1.002)	(2.761)	(171.9)	(−30.95)	(9.79)	
				MP2/6-311++G(d,p)//MP2/6-31+G(d)				
C	0					0		
CW21[d]	1/2	2.048 (2.050)	0.981 (0.981)	2.991 (2.991)	160.5 (160.1)	−10.12 (−9.98)	4.07 (4.03)	
CW11	1	1.944	0.970	2.927	174.8	−20.82	6.57	
CW12	2	1.858	0.995	2.843	170.3	−27.51	8.44	
CW13C	3	1.852	0.997	2.848	177.8	−29.83	9.03	
CW13R	3	1.891	0.991	2.880	175.5	−24.18	7.92	

[a] All ^{15}N chemical shifts are given with respect to free collidine calculated at the same level of theory, with the calculated absolute shielding of the free heterocyclic nitrogen atom of −91.54 (DFT) and −87.31 ppm (MP2). [b] ^1H chemical shifts are given with respect to calculated methane CH_4, and absolute shieldings of the protons are 31.44 (DFT) and 31.71 ppm (MP2), which has a chemical shift of 0.14 ppm[53,54] to TMS. [c] The electron density $\rho_{HN}(r)$ of the H···N bond was estimated at the critical points using the atoms-in-molecules theory of Bader with the DFT formalism. [d] Values in parentheses correspond to the second OHN hydrogen bond. Abbreviations are C for collidine and W for water.

In the presence of heterocyclic bases, water molecules may be involved in hydrogen-bonded species of different structures. Generally, the proton and hydrogen bond exchange between different acid−base complexes in solution is very fast on the NMR time scale at room temperature, which prevents identification of their structures and properties. Quite often, these exchanges can be suppressed, that is, the exchange rate becomes of the order of ms^{-1} or slower, upon cooling down to 120 K. In this case, different spectral peaks correspond to different individual species.[22−27,37] In contrast, the ^1H NMR spectra obtained for heterocycle−water mixtures display for water protons the only averaged spectral peak in the whole temperature range. The position and relative intensity of the peak depend strongly on temperature (Figure 1). At room temperature, this peak is at 2.8 ppm and is quite sharp. The position of the peak indicates that in the aprotic freonic mixtures at room temperature, water molecules spend most of the time as solitary molecules (Figure 1a). Upon cooling, water molecules become involved in more or less stable hydrogen-bonded complexes with each other and heterocycles. The exchange between different structures is still too fast to suppress averaging, but the peak becomes broader (Figure 1c). One can hardly define the most favorable structure at these temperatures. The line broadening is accompanied by a dramatic reduction of the signal relative intensity due to the water precipitation from the solution. As a result of this precipitation, the relative concentration of the base increases. Upon further cooling, the averaged ^1H chemical shift asymptotically approaches to a value of 6.7 ppm

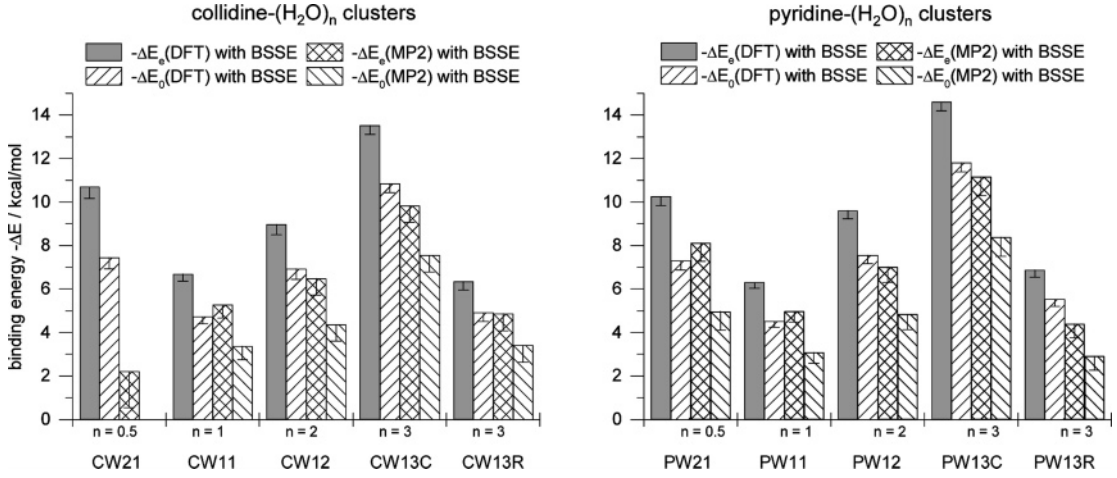

Figure 5. Schematic view of the binding energies ΔE_e of collidine− and pyridine−$(H_2O)_n$ with $n = 0.5$, 1, 2, and 3 clusters calculated at DFT and the MP2 level of theory. ΔE_0 is the ZPVE-corrected. The error bars represent the $\Delta\epsilon$(BSSE) corrections.

TABLE 2: Binding Energies of Collidine− and Pyridine−$(H_2O)_n$ Clusters with $n = 0.5$, 1, 2, 3, and 6 Calculated at DFT and the MP2 Level of Theory[a]

$n = 1$	X_2-H_2O 0.5	$X-H_2O$ 1	$X-(H_2O)_2$ 2	$X-(H_2O)_3$ 3, chain	$X-(H_2O)_3$ 3, ring	$X_2-(H_2O)_6$[b] 6, chain
X = collidine	CW21	CW11	CW12	CW13C	CW13R	CW26C
			B3LYP/6-311++G(2df,2p)//B3LYP/6-31+G(d,p)			
$-\Delta E_e^N$	10.69	6.69	8.98	13.52	6.35	15.78[c]
$-\Delta E_e^B$	10.17	6.36	8.49	13.11	5.95	14.55
$-\Delta E_0$	7.45	4.73	6.93	10.85	4.91	12.57[c]
$\Delta\epsilon$(BSSE)	0.52	0.33	0.49	0.41	0.40	1.23
			MP2/6-311++G(d,p)//MP2/6-31+G(d)			
$-\Delta E_e^N$	2.21	5.28	6.49	9.83	4.87	
$-\Delta E_e^B$	0.55	4.67	5.73	9.07	4.09	
$-\Delta E_0$	−1.52	3.37	4.37	7.54	3.41	
$\Delta\epsilon$(BSSE)	1.66	0.61	0.76	0.76	0.78	
$n = 1$	X_2-H_2O 0.5	$X-H_2O$ 1	$X-(H_2O)_2$ 2	$X-(H_2O)_3$ 3, chain	$X-(H_2O)_3$ 3, ring	$X_2-(H_2O)_6$[b] 6, chain
X = pyridine	PW21	PW11	PW12	PW13C	PW13R	PW26C
			B3LYP/6-311++G(2df,2p)//B3LYP/6-31+G(d,p)			
$-\Delta E_e^N$	10.26	6.31	9.61	14.61	6.87	17.47[c]
$-\Delta E_e^B$	9.83	6.03	9.24	14.19	6.54	16.49
$-\Delta E_0$	7.30	4.52	7.56	11.81	5.53	13.97[c]
ϵ(BSSE)	0.43	0.28	0.38	0.42	0.33	0.98
			MP2/6-311++G(d,p)//MP2/6-31+G(d)			
$-\Delta E_e^N$	9.03	5.40	7.66	11.89	5.11	
$-\Delta E_e^B$	8.17	4.90	6.94	11.01	4.47	
$-\Delta E_0$	5.87	3.51	5.49	9.11	3.61	
$\Delta\epsilon$(BSSE)	0.86	0.50	0.72	0.88	0.64	

[a] All energies are in kcal/mol. "$-\Delta E_e^N$" and "$-\Delta E_e^B$" represent the binding energy without and with the basis set superposition error correction $\Delta\epsilon$(BSSE), respectively. ΔE_0 is the ZPVE-corrected ΔE_e. The frequencies for ZPVE correction were evaluated at the MP2/6-31+G(d) and B3LYP/6-31+G(d,p) level of theory. [b] Using the double energy of the optimized water timer clustered as chain. [c] Energies are divided by two for comparison with the other clusters. Abbreviations are C for collidine, P for pyridine, and W for water.

at 130 K (cf. Figure 1f) being accompanied by a decrease of the peak widths that is indicated on the further exchange suppression. It is reasonable to assume that at these conditions the 2:1 heterocycle−water complex dominates in the solution. This interpretation will also be in agreement with results of the FT-IR studies on pyridine−water complexes.[20,21] Let us verify this assumption. In Figure 6, the correlations of the ^1H vs ^{15}N chemical shifts in the liquid state (dash line) and solid state (solid line) are presented. These correlations were established from pyridine− and collidine−carboxylic acid complexes in the highly polar freonic mixtures at low temperature and in the organic solid state.[22−24,26−28] As was described in the theoretical section, the parameter set used to calculate the curves in Figure 6 is obtained from previous work.[26] For a better comparison, it is convenient to reference the ^{15}N chemical shifts to the corresponding bulk frozen bases. The GIAO-calculated ^1H and ^{15}N chemical shifts of the model heterocyclic collidine−water clusters are also depicted in Figure 6. The calculated ^1H chemical shifts for the clusters with more than one water molecule involved are somewhat lower as compared to the solid-state correlation (Figure 6). The deviation may come from the neglect of the proton vibrational motion.[65] Besides that, it is not surprising that the theory does not precisely reflect the situation in the high polar freonic mixtures.[37] However, the calculated ^{15}N chemical shift of the CW21 cluster helps to estimate where the water signal should resonate in a polar

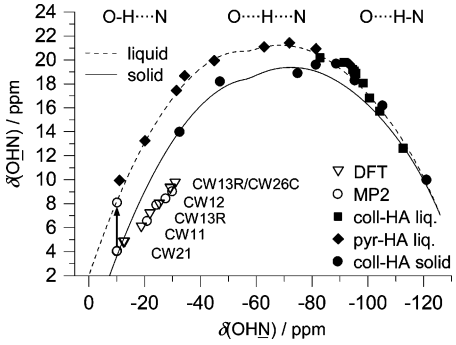

Figure 6. ^{1}H vs ^{15}N chemical shift correlation in liquid state (dash line) and solid phase (solid line). Filled diamonds and square symbols refer to pyridine− or collidine−HA complexes in freon mixtures, respectively.[22−24] The filled circles refer to the collidine−HA complexes in solid state.[28] Open symbols correspond to GIAO ^{1}H and ^{15}N chemical shifts of collidine−water clusters calculated at DFT (▽) and the MP2 (○) level of theory. The extrapolated ^{1}H chemical shift of 8.1 ppm for the CW21 cluster in freon mixtures is also shown.

freonic mixtures. The value of 8.1 ppm, which can be estimated by extrapolating it to the liquid-state curve in Figure 6, is close to the experimental limit value of 6.7 ppm.

The obtained experimental data indicate that in the aprotic freonic mixtures water can be suspended at low temperatures exclusively in the form of the symmetric 2:1 heterocycle−water complexes and demands about 20-fold base excess. This excess stimulates an exchange between free and hydrogen-bonded base molecules, which is too fast on the NMR time scale even at the lowest experimentally achievable temperature of about 100 K. Thus, the employed freonic mixtures can hardly be used to study more complex biologically relevant hydrogen-bonded water bridges.

Water−Base Complexes in Solid State. Recently, some of us have shown that the NMR parameters correlate with the geometries of the OHN hydrogen bonds.[26−28] We prefer to discuss the experimental data obtained for collidine since its hydrogen-bonded complexes were recently extensively studied.[22−24,28] The correlation curves shown in Figure 7a were established from neutron diffraction geometries.[57,58] The dotted line in Figure 7a represents the correlation between $q_2 = r_{OH} + r_{HN}$ and $q_1 = 1/2\ (r_{OH} - r_{HN})$, which refer to the equilibrium geometries where the zero-point vibrations are not taken into account. The experimental data were analyzed with a more accurate empirical correction where the zero-point motions were included (solid line in Figure 7a). We note that the optimized geometries of the collidine−water clusters (Figure 7a) calculated using the DFT and MP2 level of theory are well-located on the correlation curves, which validates our theoretical calculations.

Experimentally, two hydrogen-bonded species in the frozen phase of heterocyclic bases−water complexes were identified. The first one was observed when the heterocyclic base was in excess while the second one was observed when water was in excess. In the case of collidine, these species resonate at −11 (collidine excess) and −23 ppm (water excess) with respect to the frozen bulk collidine. Theoretical studies indicate that when the base is in excess the most energetically stable structure is the 2:1 heterocycle−water cluster, where one water is coordinated to two bases. Here, we will call this complex as "symmetric". When water is in excess, the most energetically stable structure represents the longest possible water chain coordinated to two bases. However, a closer look in Tables 1 and 2 shows that both the length of the N···H bond and the energy of CW13C and CW26C clusters are very similar. Thus, as soon as collidine is bound to a water chain, which includes

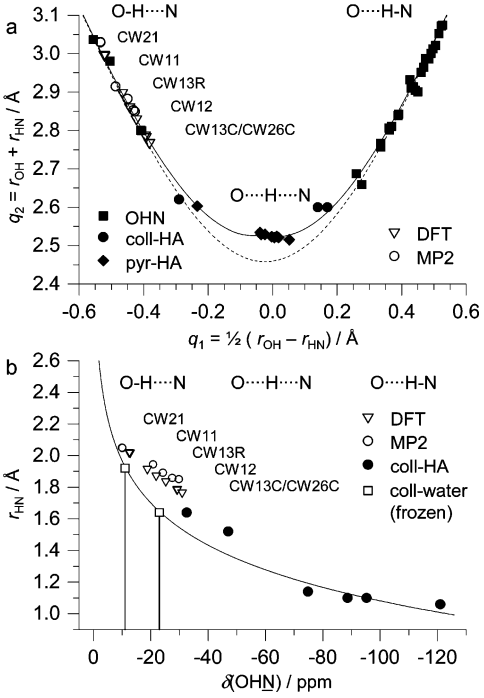

Figure 7. Geometric OHN hydrogen bond correlation of collidine−water clusters. (a) q_2 vs q_1. Equilibrium (dotted) and corrected (solid) correlation curves were calculated according to ref 26. Filled symbols refer to neutron diffraction geometries.[57,58] Open symbols respond to optimized geometries of collidine−water clusters calculated at DFT (▽) and MP2 (○) level of theory. (b) NH distance vs ^{15}N chemical shift correlation. ● represents the obtained r_{HN} distances for collidine−HA complexes by dipolar solid-state NMR,[28] with respect to the frozen bulk collidine. □ represents the estimated r_{HN} distances by NMR of the frozen collidine−water complexes at −11 (2:1) and −23 ppm (1:3); they are $r_{HN} = 1.92$ and 1.64 Å, $r_{OH} = r_{NO} - r_{HN} = 0.98$ and 1.03 Å, respectively. For the calculation of the correlation curves, see the text.

more than two water molecules, the ^{15}N NMR chemical shift should become insensitive to the presence or absence of any other water or base molecules on the opposite end of the chain. Here, we will call such complexes "asymmetric", keeping in mind that all of what we know about them is that they contain a water bridge formed by more than two water molecules terminated on one end with collidine.

From the ^{15}N chemical shifts of the ring nitrogen, involved in the intermolecular OHN hydrogen bond to water, it is possible to obtain the corresponding r_{HN} distances using the established correlation (Figure 7b).[26,28] The ^{15}N chemical shift of −11 ppm corresponds to a r_{HN} distances of 1.92 Å and the shift of −23 ppm to a distance of 1.64 Å. Also, we can estimate for these species an associated apparent pK_a value of the water hydroxyl group bound to collidine. In the asymmetric complex, this hydroxyl group is "acidic" and is associated to the apparent pK_a value of about 4.9. In the symmetric complex, it is less "acidic" and the associated apparent pK_a is about 6.0. The interested reader can find the plot of the pK_a values as a function of the ^{15}N chemical shifts in the Supporting Information. Note that we also found these two species for the frozen pyridine−water mixtures, which resonated at −14 and −20 ppm with respect to the frozen bulk pyridine. In the case of pyridine, these chemical shifts correspond to r_{HN} distances of 1.82 Å for −14 ppm and 1.69 Å for −20 ppm.

In the asymmetric species, the outer water molecule bonded to the base is also bonded to other water molecules. When the OHN hydrogen bond becomes shorter, the coupled OHO hydrogen bond becomes shorter as well. One speaks about the

cooperative interaction of hydrogen bonds. Hence, the proton-donating ability of the water molecule bonded to the base increases due to this mutual cooperative interaction with other water molecules and is associated in the case of collidine with an apparent pK_a value of about 4.9. In contrast, in the symmetric species, the water molecule is bonded to two equal heterocyclic bases. Thus, a shortening of one OHN hydrogen bond results in a lengthening of the other. One speaks about the anticooperative interaction. Hence, the proton-donating ability of water in the symmetrical collidine species decreases due to the anticooperative interaction that is reflected by an associated apparent pK_a value of about 6.0.

The experimental findings show differences in the OHN hydrogen bond geometries of the heterocyclic base−water complexes depending on whether pyridine or its trimethyl derivative collidine is involved. In the symmetric species, where one water molecule is bounded to two bases, the longer r_{HN} distance of 1.92 Å for collidine in comparison to the shorter r_{HN} distance of 1.82 Å for pyridine can be explained by the steric hindrance of the *ortho*-methyl groups of collidine. The steric repulsion of the methyl groups weakens the hydrogen bond interaction in this complex. The opposite behavior is observed for the asymmetric species where the base is bounded to a water bridge. A shorter r_{HN} distance of 1.64 Å for collidine in comparison to the longer r_{HN} distance of 1.69 Å for pyridine is found. This can be explained by the stronger basicity[60] of the collidine.

Conclusion

The main goals of this work were experimental simulation and property analyses of water hydrogen-bonded bridges terminated by heterocyclic bases. Such species are relevant for many biological systems. It was shown that aprotic freonic mixtures extensively used in the past to analyze the composition and geometry of hydrogen-bonded complexes were not suitable to study these kinds of water bridges. Below 170 K, water precipitated from the solvent. About 20-fold excess of the base was needed to suspend water in the aprotic mixture at lower temperatures. As a result, only the simplest form of such a bridge, namely, one water molecule coordinated to two bases, was experimentally detected at these conditions. A complex of the same structure was experimentally observed in frozen heterocycle−water solutions when the base was in excess. The proton-donating ability of water in these complexes was affected by an anticooperative interaction between the two mutually coupled hydrogen bonds and corresponded to an apparent pK_a value of about 6.0. Species of a more complex structure were identified in frozen heterocycle−water solutions when water was in excess. Model theoretical calculations predicted that such species should contain a heterocyclic base bound to a water chain. Although the length of the N···H bond in such complexes became shorter while the length of the water bridge increased, the amplitude of these changes was quite small. Thus, the effect of the shortening was not detected experimentally in ^{15}N NMR spectra upon a gradual increase of the water/base ratio in the mixture. At the same time, such species, containing more than two mutually bound water molecules with one of them bound to the heterocyclic base, represent an example of the required biologically relevant bridges. The proton-donating ability of the hydroxyl group bound to the base in such chains was increased as compared to the simplest 2:1 heterocycle−water cluster due to a cooperative interaction with other water molecules forming the chain. As a result, the proton-donating ability of the terminal hydroxyl group corresponded to an associated apparent pK_a value of about 4.9. It seems that this value depends only slightly on the length of the water bridge and on the presence of another base at the other end of the bridge if more than two water molecules are involved.

Thus, the main conclusion of this work is that the proton-donating ability of the outer hydroxyl groups of a water chain involved more than two molecules is not measurable depending on the chain length and is comparable to the proton-donating ability of a fictitious acid exhibiting a pK_a value of about 4.9 in water.

Acknowledgment. This work was supported by the Deutsche Forschungsgemeinschaft, Bonn; the Fonds der Chemischen Industrie, Frankfurt; the Russian Ministry of Education and Science (project RNP 2.1.1. 4139); and the Russian Foundation of Basic Research (project 05-03-33235). L.G. thanks "Berliner Förderungsprogramm" for financial support. The Hochschulrechenzentrum FU Berlin is gratefully acknowledged for the allocation of computational time.

Supporting Information Available: ^{1}H NMR spectra of a mixture of ^{15}N labeled pyridine with water in freon mixture. ^{15}N NMR spectra of the heterocyclic−water mixtures in liquid state. MP2 optimized structures of the pyridine−water clusters. The plot of the pK_a values as a function of the ^{15}N chemical shifts. Full details of NMR and selected structural H-bonds parameters of collidine− and pyridine−water clusters. This material is available free of charge via the Internet at http://pubs.acs.org.

References and Notes

(1) Smedarchina, Z.; Siebrand, W.; Fernandez-Ramos, A.; Cui, Q. *J. Am. Chem. Soc.* **2003**, *125*, 243−251.

(2) Smedarchina, Z.; Fernandez-Ramos, A.; Siebrand, W. *J. Comput. Chem.* **2001**, *22*, 787−801.

(3) Smedarchina, Z.; Siebrand, W.; Fernandez-Ramos, A.; Gorb, L.; Leszczynski, J. *J. Chem. Phys.* **2000**, *112*, 566−573.

(4) Mori, K.; Ogawa, Y.; Ebihara, K.; Tamura, N.; Tashiro, K.; Kuwahara, T.; Mukoyama, M.; Sugawara, A.; Ozaki, S.; Tanaka, I.; Nakao, K. *J. Biol. Chem.* **1999**, *274*, 15701−15705.

(5) Duda, D.; Tu, C.; Silverman, D. N.; Kalb, A. J.; Agbandje-McKenna, M.; McKenna, R. *Protein Pept. Lett.* **2001**, *8*, 63−67.

(6) Duda, D.; Govindasamy, L.; Agbandje-McKenna, M.; Tu, C.; Silverman, D. N.; McKenna, R. *Acta Crystallogr. D* **2003**, *D59*, 93−104.

(7) Tu, C.; Rowlett, R. S.; Tripp, B. C.; Ferry, J. G.; Silverman, D. N. *Biochemistry* **2002**, *41*, 15429−15435.

(8) Silverman, D. N.; Lindskog, S. *Acc. Chem. Res.* **1988**, *21*, 30−36.

(9) An, H.; Tu, C.; Duda, D.; Montanez-Clemente, I.; Math, K.; Laipis, P. J.; McKenna, R.; Silverman, D. N. *Biochemistry* **2002**, *41*, 3235−3242.

(10) Riehn, C.; Reimann, B.; Buchhold, K.; Vaupel, S.; Barth, H. D.; Brutschy, B.; Tarakeshwar, P.; Kim, K. S. *J. Chem. Phys.* **2001**, *115*, 10045−10047.

(11) Tarakeshwar, P.; Kim, K. S.; Djafari, S.; Buchhold, K.; Reimann, B.; Barth, H. D.; Brutschy, B. *J. Chem. Phys.* **2001**, *114*, 4016−4024.

(12) Tarakeshwar, P.; Kim, K. S.; Brutschy, B. *J. Chem. Phys.* **2001**, *114*, 1295−1305.

(13) Tarakeshwar, P.; Kim, K. S.; Brutschy, B. *J. Chem. Phys.* **2000**, *112*, 1769−1781.

(14) Tarakeshwar, P.; Kim, K. S.; Brutschy, B. *J. Chem. Phys.* **1999**, *110*, 8501−8512.

(15) Luchow, A.; Spangenberg, D.; Janzen, C.; Jansen, A.; Gerhards, M.; Kleinermanns, K. *Phys. Chem. Chem. Phys.* **2001**, *3*, 2771−2780.

(16) Gerhards, M.; Jansen, A.; Unterberg, C.; Kleinermanns, K. *Chem. Phys. Lett.* **2001**, *344*, 113−119.

(17) Kleinermanns, K.; Janzen, C.; Spangenberg, D.; Gerhards, M. *J. Phys. Chem. A* **1999**, *103*, 5232−5239.

(18) Jacoby, C.; Roth, W.; Schmitt, M.; Janzen, C.; Spangenberg, D.; Kleinermanns, K. *J. Phys. Chem. A* **1998**, *102*, 4471−4480.

(19) Papai, I.; Jancso, G. *J. Phys. Chem. A* **2000**, *104*, 2132−2137.

(20) Wolff, H.; Hagedorn, W.; Mathias, D.; Rethel, R.; Millermann, E.; Leidner, L. *J. Phys. Chem.* **1978**, *82*, 2404−2409.

(21) Destexhe, A.; Smets, J.; Adamowicz, L.; Maes, G. *J. Phys. Chem.* **1994**, *98*, 1506−1514.

(22) Tolstoy, P. M.; Smirnov, S. N.; Shenderovich, I. G.; Golubev, N. S.; Denisov, G. S.; Limbach, H.-H. *J. Mol. Struct.* **2004**, *700*, 19−27.
(23) Smirnov, S. N.; Benedict, H.; Golubev, N. S.; Denisov, G. S.; Kreevoy, M. M.; Schowen, R. L.; Limbach, H.-H. *Can. J. Chem.* **1999**, *77*, 943−949.
(24) Smirnov, S. N.; Golubev, N. S.; Denisov, G. S.; Benedict, H.; Schah-Mohammedi, P.; Limbach, H.-H. *J. Am. Chem. Soc.* **1996**, *118*, 4094−4101.
(25) Golubev, N. S.; Denisov, G. S.; Smirnov, S. N.; Shchepkin, D. N.; Limbach, H.-H. *Z. Phys. Chem.* **1996**, *196*, 73−84.
(26) Limbach, H.-H.; Pietrzak, M.; Sharif, S.; Tolstoy, P. M.; Shenderovich, I. G.; Smirnov, S. N.; Golubev, N. S.; Denisov, G. S. *Chem. Eur. J.* **2004**, *10*, 5195−5204.
(27) Limbach, H.-H.; Pietrzak, M.; Benedict, H.; Tolstoy, P. M.; Golubev, N. S.; Denisov, G. S. *J. Mol. Struct.* **2004**, *706*, 115−119.
(28) Lorente, P.; Shenderovich, I. G.; Golubev, N. S.; Denisov, G. S.; Buntkowsky, G.; Limbach, H.-H. *Magn. Reson. Chem.* **2001**, *39*, S18−S29.
(29) Shenderovich, I. G.; Buntkowsky, G.; Schreiber, A.; Gedat, E.; Sharif, S.; Albrecht, J.; Golubev, N. S.; Findenegg, G. H.; Limbach, H.-H. *J. Phys. Chem. B* **2003**, *107*, 11924−11939.
(30) Del Bene, J. E.; Elguero, J. *J. Phys. Chem. A* **2006**, *110*, 1128−1133.
(31) Del Bene, J. E.; Elguero, J. *J. Phys. Chem. A* **2005**, *109*, 10759−10769.
(32) Del Bene, J. E.; Elguero, J. *J. Phys. Chem. A* **2005**, *109*, 10753−10758.
(33) Del Bene, J. E.; Perera, S. A.; Bartlett, R. J.; Yáñez, M.; Mó, O.; Elguero, J.; Alkorta, I. *J. Phys. Chem. A* **2003**, *107*, 3121−3125.
(34) Del Bene, J. E.; Bartlett, R. J.; Elguero, J. *Magn. Reson. Chem.* **2002**, *40*, 767−771.
(35) Golubev, N. S.; Smirnov, S. N.; Schah-Mohammedi, P.; Shenderovich, I. G.; Denisov, G. S.; Gindin, V. A.; Limbach, H.-H. *Russ. J. Gen. Chem.* **1997**, *67*, 1082−1087.
(36) Siegel, J. S.; Anet, F. A. L. *J. Org. Chem.* **1988**, *53*, 2629−2630.
(37) Shenderovich, I. G.; Burtsev, A. P.; Denisov, G. S.; Golubev, N. S.; Limbach, H.-H. *Magn. Reson. Chem.* **2001**, *39*, S91−S99.
(38) Hayashi, S.; Hayamizu, K. *Bull. Chem. Soc. Jpn.* **1991**, *64*, 688−690.
(39) Møller, C.; Plesset, M. S. *Phys. Rev.* **1934**, *46*, 618−622.
(40) Head-Gordon, M.; Pople, J. A.; Frisch, M. J. *Chem. Phys. Lett.* **1988**, *153*, 503−506.
(41) Becke, A. D. *J. Chem. Phys.* **1993**, *98*, 5648−5652.
(42) Lee, C.; Yang, W.; Parr, R. G. *Phys. Rev.* **1988**, *B37*, 785−789.
(43) Hariharan, P. C.; Pople, J. A. *Theor. Chim. Acta* **1973**, *28*, 213−222.
(44) Krishnan, R.; Binkley, J. S.; Seeger, R.; Pople, J. A. *J. Chem. Phys.* **1980**, *72*, 650−654.
(45) González, L.; Mó, O.; Yáñez, M. *J. Chem. Phys.* **1998**, *109*, 139−150.
(46) González, L.; Mó, O.; Yáñez, M.; Elguero, J. *J. Mol. Struct. Theochem.* **1996**, *371*, 1−10.
(47) Boys, S. F.; Bernardi, F. *Mol. Phys.* **1970**, *19*, 553−566.
(48) Kim, K. S.; Tarakeshwar, P.; Lee, J. Y. *Chem. Rev.* **2000**, *100*, 4145−4185.
(49) van Duijneveldt, F. B.; van Duijneveldt-van de Rijdt, J. G. C. M.; van Lenthe, J. H. *Chem. Rev.* **1994**, *94*, 1873−1885.
(50) Bader, R. F. W. *Atoms in Molecules. A Quantum Theory*; Oxford University Press: Oxford, 1990.
(51) González, L.; Mó, O.; Yáñez, M.; Elguero, J. *J. Chem. Phys.* **1998**, *109*, 2685−2693.
(52) Wolinski, K.; Hinton, J. F.; Pulay, P. *J. Am. Chem. Soc.* **1990**, *112*, 8251−8260.
(53) Zuschneid, T.; Fischer, H.; Handel, T.; Albert, K.; Haefelinger, G. *Z. Naturforsch. B* **2004**, *59*, 1153−1176.
(54) Kutzelnigg, W.; Fleischer, U.; Schindler, M. In *NMR Basic Principles and Progress*; Diehl, P., Fluck, E., Kosfeld, R., Eds.; Springer: Berlin, 1990; Vol. 23, pp 165−262.
(55) Frisch, M. J.; Trucks, G. W.; Schlegel, H. B.; Scuseria, G. E.; Robb, M. A.; Cheeseman, J. R.; Zakrzewski, V. G.; Montgomery, J. A., Jr.; Stratmann, R. E.; Burant, J. C.; Dapprich, S.; Millam, J. M.; Daniels, A. D.; Kudin, K. N.; Strain, M. C.; Farkas, O.; Tomasi, J.; Barone, V.; Cossi, M.; Cammi, R.; Mennucci, B.; Pomelli, C.; Adamo, C.; Clifford, S.; Ochterski, J.; Petersson, G. A.; Ayala, P. Y.; Cui, Q.; Morokuma, K.; Malick, D. K.; Rabuck, A. D.; Raghavachari, K.; Foresman, J. B.; Cioslowski, J.; Ortiz, J. V.; Stefanov, B. B.; Liu, G.; Liashenko, A.; Piskorz, P.; Komaromi, I.; Gomperts, R.; Martin, R. L.; Fox, D. J.; Keith, T.; Al-Laham, M. A.; Peng, C. Y.; Nanayakkara, A.; Gonzalez, C.; Challacombe, M.; Gill, P. M. W.; Johnson, B. G.; Chen, W.; Wong, M. W.; Andres, J. L.; Head-Gordon, M.; Replogle, E. S.; Pople, J. A. *Gaussian 98*; Gaussian, Inc.: Pittsburgh, PA, 1998.
(56) Pauling, L. *J. Am. Chem. Soc.* **1947**, *69*, 542−553.
(57) Steiner, T.; Majerz, I.; Wilson, C. C. *Angew. Chem., Int. Ed.* **2001**, *40*, 2651−2654.
(58) Steiner, T. *J. Phys. Chem. A* **1998**, *102*, 7041.
(59) Brown, I. D. *Acta Crystallogr.* **1992**, *B48*, 553−572.
(60) Tamres, M.; Searles, S.; Leighly, E. M.; Mohrman, D. W. *J. Am. Chem. Soc.* **1954**, *76*, 3983−3985.
(61) Mó, O.; Yáñez, M.; Elguero, J. *J. Chem. Phys.* **1992**, *97*, 6628−6638.
(62) Cerny, J.; Hobza, P. *Phys. Chem. Chem. Phys.* **2005**, *7*, 1624−1626.
(63) Hobza, P.; Šponer, J.; Reschel, T. *J. Comput. Chem.* **1995**, *16*, 1315−1325.
(64) Nakahara, M.; Wakai, C. *Chem. Lett.* **1992**, *5*, 809−812.
(65) Del, Bene, J. E.; Jordan, M. J. T. *J. Phys. Chem. A* **2002**, *106*, 5385−5392.